The Pennsylvania State University

The Graduate School

Department of Mechanical and Nuclear Engineering

BLAST MITIGATION STUDIES FOR ALL METAL PLATE AND HONEYCOMB SANDWICH PANELS

A Thesis in

Mechanical Engineering

by

Anand Kumar Singh

Submitted in Partial Fulfillment
of the Requirements
for the Degree of

Master of Science

May 2012

The thesis of Anand Kumar Singh was reviewed and approved* by the following:

Ashok D. Belegundu
Professor of Mechanical Engineering
Thesis Advisor

Timothy W. Simpson
Professor of Mechanical Engineering and Industrial Engineering
and Engineering Design
Director of Learning Factory

Karen A. Thole
Professor of Mechanical Engineering
Head of the Department of Mechanical and Nuclear Engineering

*Signatures are on file in the Graduate School

ABSTRACT

This thesis investigates the optimization of a solid all-metal plate and a honeycomb sandwich panel to mitigate the effect of air blast loading, which consists of a short duration pressure pulse. With respect to the all-metal aluminum plate, the focus is on studying convergence of shape with regard to increasing number of velocity fields, well-posedness of the problem and effects of the different boundary conditions and off-center charge locations. The plates are modeled using LS-DYNA with 3-D hexahedral elements. The goal is to minimize the peak dynamic displacement of the back-face while monitoring plastic strain values, mass, and envelope constraints. Robust convergence of the numerical procedure is shown, as also the well-posedness of the problem formulation. A study with different boundary conditions along the edge has also been performed. The change in the optimized shape of the plate as the charge migrates away from the center is also studied.

With respect to the honeycomb sandwich panel, the focus is to validate the homogenized stress-strain curve obtained via virtual testing of the unit cell. To this end, a large scale virtual crush test is performed on a detailed finite element model of the honeycomb to obtain a stress-strain curve. This curve shows good agreement with the parameterized curve used in homogenization. As the honeycomb core in sandwich panel flexes under the blast load, virtual three-point bending tests are also performed on the detailed finite element model of the sandwich panel. Deflection response, stiffness values and energy captured by the sandwich are then compared with corresponding values for the homogenized model.

TABLE OF CONTENTS

LIST OF FIGURES

LIST OF TABLES

ACKNOWLEDGEMENTS

Financial and computational support from the Research Computing and Cyberinfrastructure group, a unit of ITS Penn State under Mr. Vijay Agarwala, is gratefully acknowledged.

Chapter 1

Introduction

1.1 Overview

Today explosives find use in a broad range of martial and civil applications. Explosions produce high accelerations which can create direct shock and injury, generate flying debris, and damage electronics. Therefore, safety is of prime concern both during the use and storage of explosives. The goal of this research is to mitigate the shock transmitted through a protective panel by minimizing the dynamic deflection into the protected space, and the transmitted accelerations. To this end the optimization of panel geometry and properties of the core of a sandwich panel is pursued in this research. The work is relevant to design of land and marine vehicles, helmets and other commercial applications.

This thesis represents the actual contribution of the author towards a group project, involving other researchers, on design of panels for blast load mitigation. The work done by the author addresses two separate topics:

1. Optimization of all-metal plates, considering convergence of shape with respect to increasing number of velocity fields, well-posedness, boundary conditions and charge locations (Chapter 2), and

2. Homogenization of the constitutive law for a honeycomb sandwich panel. This work paves the way for subsequent optimization of the honeycomb sandwich (Chapter 3).

The design problem is as follows. The panel is subjected to a blast load of specified magnitude at a given standoff distance. We denote the face of the panel that faces the blast

pressure as the ‘front-face’, and the backside as the ‘back-face’. Since the z-direction points away from the charge, the front-face is also referred to as the ‘bottom’ and the back-face as the ‘top’. Thus, for instance, bottom bulge is a bulge of the face that faces the charge. In the context of vehicle design, the back-face is on the cabin or occupant side while the front-face is nearer to the ground. The effect of the blast is expressed as a pressure-time load on the front-face.

For the all-metal panel, the project goal is to optimize size and shape to minimize the back-face deflection. This amounts to increase in the stiffness of the plate, reduced indentation and lighter structure having adequate protection. Work items involved in the all-metal panel optimization are given below. The items are comprehensive with regard to the entire project, and specific contributions made by the author are indicated in parenthesis as ‘author’ while remaining items are referred to the publications of co-researchers.

All-metal panel

Item 1. Definition of the design optimization problem [14]

Item 2. Development of FE model using LS-DYNA. Note that LS-DYNA was chosen owing to its built-in capability to generate the pressure-time load from blast data [14]

Item 3. Development of FORTRAN program to implement Differential Evolution (DE) for parallel computing [14]

Item 4. Sizing the plate thickness and optimizing the face-plate shapes to minimize the back-face deflection for a *centrally* located charge [14]

Item 5. Sizing the plate thickness and optimizing the face-plate shapes to minimize the back-face deflection for varying offset locations of the charge (author)

Item 6. Study of the effect of different panel boundary conditions, viz. all edges fixed, all edges pinned, a freely suspended grip system (author)

Item 7. Well-posedness of the problem, meaning whether the optimized results are obtainable and the same from different starting shapes (author)

Item 8. Convergence of the optimized shape with increasing number of basis shapes (author)

For the honeycomb sandwich panel, the project goal is to minimize both back-face deflection and back-face acceleration, the latter possible owing to the energy absorbing potential within the honeycomb core. Work items involved in the honeycomb sandwich panel optimization are given below.

Honeycomb sandwich panel

Item 1. Unit cell testing [11]

Item 2. Homogenization based on Item 1 [11]

Item 3. Validation

(a) Comparison to literature (Wierzbicki [8]) [11]

(b) Validation with detailed crush model (author)

Item 4. Behavior of beam models for multiaxial loading (author)

Item 5. The sizing optimization problem definition [11]

Item 6. Code modifications to accept honeycomb material design variables (author)

The author's contribution to all-metal panel are detailed in Chapter 2 and the work items related to honeycomb sandwich panel are given in Chapter 3.

1.2 Problem Definition for All-Metal Plate

Mathematically, the design optimization problem can be stated as follows:

Minimize	$max\ \delta_b$	
subject to	$\varepsilon_{pj} \leq \varepsilon_{\text{pmax}}$	for each element j in the all-metal plate
	$M \leq M_{\max}$	
	$t \geq t_{\min}$	
	$\mathbf{x}^{\text{L}} \leq \mathbf{x} \leq \mathbf{x}^{\text{U}}$	
	$det\ J_j(\mathbf{x}) \geq 0$	for each element j
	$\mathbf{z}^{\text{L}} \leq \mathbf{z} \leq \mathbf{z}^{\text{U}}$	(envelope)

where

(i) δ_b , the objective function, is taken equal to the root mean square (RMS) value of the z-displacement of nodes in the plate taken relative to the stiffener (if any). The displacement is a function of time, and the value at the first peak is monitored.

(ii) Plastic strain, ε_p, also a function of time, stabilizes after a certain simulation time duration. This stabilized value is used in the constraint.

(iii) Thickness t is computed from nodal coordinates of the hexahedral elements used in the FE model. Element distortion is prevented by computing determinant of Jacobian J in every element and is forced to stay positive during optimization.

(iv) The mass of the assembly M is kept below a maximum limit. The design variables $\mathbf{x}$ are maintained within bounds. The design variables are the velocity fields used to change the shape of the plate. The optimized plate also has to fit within an envelope.

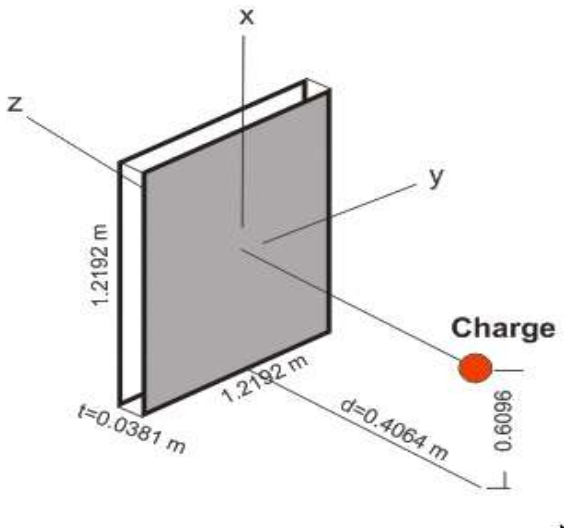

Figure 1-1. Schematic representation of a flat all-metal plate being subjected to a blast load

Fig. 1-1 shows an initially flat all-metal plate in the setup used for the optimization. This thesis focuses on various aspects of this optimization procedure like convergence of the shape with regard to increasing number of velocity fields, well-posedness of the problem, and the effect of different boundary conditions and off-center charge locations.

1.3 Problem Definition for the Honeycomb Sandwich Panel

Virtual testing of the unit cell (see Fig. 1-2) gives a stress-strain curve for the honeycomb core. This, however, is based on uniaxial compression only. Since the blast panel experiences a broader range of deformation modes, it is necessary to validate the aforementioned stress-strain curve.

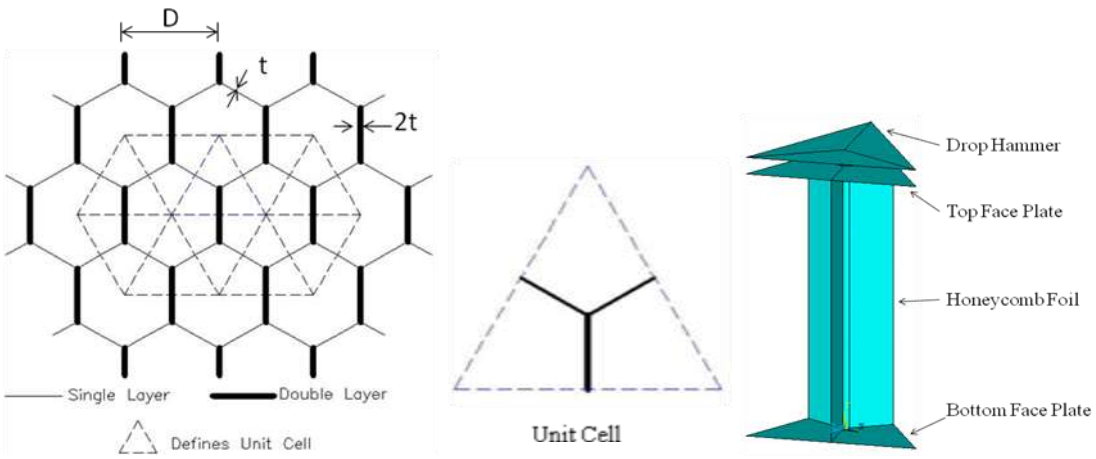

Figure 1-2. (a) Honeycomb cell geometry (b) Unit cell (c) Unit cell used in uniaxial crushing

The following questions arise when the stress-strain curve obtained from a uniaxial test on a unit cell is used to model the behavior of a sandwich panel consisting of multiple unit cells under multiaxial loading:

- Accuracy of the parameterized curve obtained from the unit cell in representing the crushing of the honeycomb core
- Adequacy of the homogenized material in characterizing the behavior of the material in both orientations of the honeycomb ribbon
- Ability of the homogenized material to simulate the behavior of the actual material in flexure

This thesis attempts to answer these questions.

1.4 Literature Research

Considerable attention in journals and conferences worldwide has been given to *analysis* of metallic and composite panels, subject to both blast and ballistic loads. Regarding *design* for impact mitigation, much greater focus has been placed on ballistic impact rather than on blast. Very few papers use formal optimization techniques. Dharaneepathy and Sudhesh [1] investigate

stiffener patterns on a square plate and demonstrate that stiffeners do provide significant advantage compared to an un-stiffened panel of same weight, and that a waffle pattern is not as good. Failure was not considered in their study – that is, only deflection was considered. Xue and Hutchinson [2] and Fleck and Deshpande [3] compare blast resistance of solid versus sandwich panels and concluded that some of the sandwich topologies outperformed solid panels of the same mass, especially in water. The plates were considered to be infinitely long in one direction and fixed at the ends of the short direction. Xue and Hutchinson [2] used Abaqus/Explicit to model the blast load while an approximate analytical approach was used by Fleck and Deshpande [3]. Highly refined three-dimensional finite element model of the sandwich plate is used to compute the blast resistance followed with an attempt to optimize to achieve maximum performance at a specified weight in [2]. This work also attempts to find near-optimization design of sandwich structures of similar properties (which are typically represented by dimensionless parameters like mass per unit area). However, no formal optimization methodology is considered. Yen, Skaggs and Cheeseman [4] indicate that significant reduction in the maximum stress amplitude propagating within the protected components can be achieved by suitable selection of a honeycomb material with proper crush strength. This work establishes the use of blast load within LS-DYNA for a reasonable accuracy. Main and Gazonas [5] study the effect of an air blast on uniaxial crushing of a cellular sandwich plates. They discuss one-dimensional systems with different boundary conditions considered in previous studies. Argod, et al. [6] focused on shape optimization for blast loading of a particular plate in a grip system. The bottom bulge in all-metal panels has been experimentally arrived at in [14]. There are instances in the public domain that show the mitigating effects of the shape of the plate. For example, United States Patent 7357062 (http://www.freepatentsonline.com/7357062.html) shows that a V-shape deflects blast waves away.

In this thesis, questions relating to convergence of shape with respect to increasing number of basis shapes, well-posedness of the problem, and boundary conditions are studied in detail. To date, design optimization is based more on approximate models as opposed to detailed capture of the response via 3D finite elements coupled to optimizers. With reference to honeycomb sandwich panels, scarce attention has been given to the homogenization of material constitutive law for optimization of nonlinear structural response. A validation procedure based on virtual testing, as presented here, is a new process in the field.

Chapter 2

All-Metal Solid Plate

2.1 Optimizer

During computational experiments, it was observed when using a gradient-based optimizer, downhill or descent search directions did not always lead to a reduction in the objective function even for small steps. The problem was seen to be clearly non-differentiable, attributable to the dynamic nature of the response. Hence use of gradient based optimizers is not appropriate. The Differential Evolution (DE) technique has proven successful [15]. DE is similar to genetic algorithms in some respects such as involving a population of designs and having generations. DE requires fewer control variables, is robust and is very well designed for parallel computation implementation. Decision parameters of the algorithm are mutation scaling factor and cross over factor for the generation of a population during a new generation. Here, random scaling factor was used for the linear crossover combination of best member and older population, for better diversity. Penalty approach was used to satisfy the constraints. Quadratic external penalty function was used for plastic strain, geometric and mass constraints, while violation of Jacobian constraint was handled by returning a very high function value since finite element analysis cannot be carried out with a distorted mesh. The total number of LS-DYNA runs is the product of population size and the number of generations. Since DE is stochastic in nature, different seeds have been tried and the best answer based on the minimum objective function value was chosen. Parallelization of the DE optimizer makes it viable to directly optimize with accurate LS-DYNA FE model response.

The population size was set equal to ten times the number of design variables as a rule of thumb. The number of generations varied from 30 to 60 depending upon the number of design variables being solved for, population size and complexity of the optimization problem (charge location, boundary conditions, etc.). As each function evaluation (LS-DYNA run) involved a new shape the computation time varied between 90 secs. to 6 mins. This put the total time for a typical optimization run around 120 hours on a single processor corresponding to 1500 LS-DYNA runs. To save computation time, analysis of a population of designs was distributed to nodes in a multi-processor computing cluster. A FORTRAN computer program with MPI calls has been developed [14]. The LION-XC and LION-XI clusters at the Pennsylvania State University's Research Computing and Cyberinfrastructure (RCC) were used.

Fig. 2-1 shows the convergence of the objective function value over the course of a single optimization run. A 4 design variable (4-DV) honeycomb size and material optimization problem with a population of 50 was run for 30 generations in 18 hours on 8 processors.

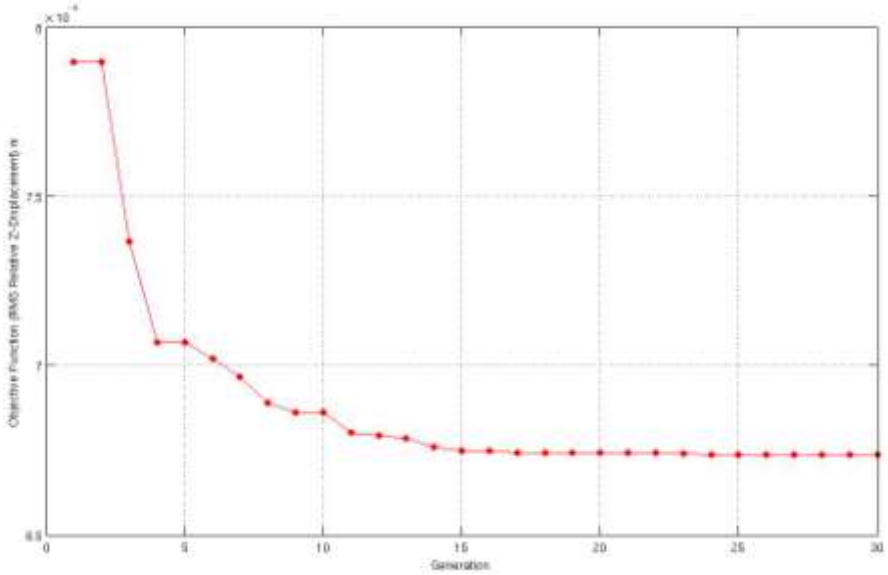

Figure 2-1. Convergence of objective function value over a single optimization run

Coordinate files are written for every population generated and checked for distortion of the mesh. High function value is returned for a distorted mesh; otherwise the LS-DYNA solver is invoked. DYNA writes nodal and element related time history outputs to ASCII files called ‘nodout’ and ‘elout’ respectively. FORTRAN routines are written to open these files and calculate relative displacement values and constraint values which are added to objective function as quadratic penalties. Based on the objective function values of all the population members and previous generations, best member is selected and stored. After the last generation, best member is written to the output file along with max displacement value and values of plastic strain. The visualization of the results is through LS-Prepost.

2.2 Determination of Well-posedness of the Optimization Problem

It is necessary to verify that the same optimization results are obtained regardless of the starting point. Specifically, if the optimized shape is a convex double bulge, then it is necessary to verify whether this same shape is obtained when the initial shape is flat and feasible, flat and infeasible, a concave double bulge, etc. This question pertains to both the formulation of the problem and to the optimization algorithm. To investigate this well-posedness of the problem numerically, initial shapes violating the constraints were put through the optimization routine. The problem is optimized using three design variables or the 3-DV case. In each case a population of 30 is iterated through 60 generations to reach the optimum.

Case 1: Initial Shape Violating Mass and Envelope Constraints

A flat plate is taken as the initial shape (see Fig. 2-2) with enough thickness to exceed the mass constraint and simultaneously breach both the upper and lower envelope constraints as can

be seen in Table 2-1. A feasible optimum, satisfying all the constraints is obtained. The optimized shape is shown in Figure 2-3, and the results are included in Table 2-1.

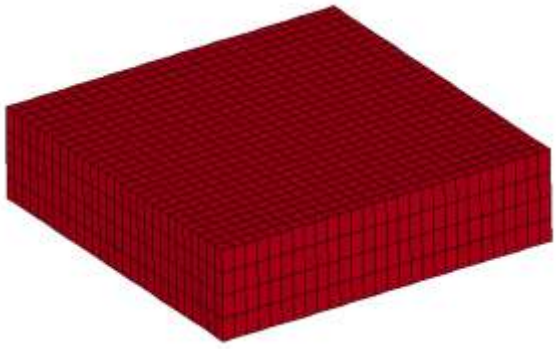

Figure 2-2. Initial shape for Case 1

Figure 2-3. Optimized shape for Case 1

Table 2-1. Results for Initial and Optimized Shape of Case 1

Parameter	Initial Shape	Optimized Shape
Objective Function (*m*)	6538	4.483×10^{-3}
Mass of the Assembly (*kg*)	3619.76	1893.67
Maximum Z-coordinate (*m*)	0.1774	0.1381
Minimum Z-coordinate (*m*)	-0.1393	-0.0995
Maximum Plastic Strain	0.00	0.02088
Minimum thickness (*m*)	0.3168	0.0235

Case 2: Initial Shape Violating Minimum Thickness and Plastic Strain Constraints

A plate thinner than the minimum allowed thickness (see Fig. 2-4) is taken and consequently the plastic strain limit is also violated. The optimizer corrects the violation (see Fig. 2-5). Results are summarized in Table 2-2.

Figure 2-4. Initial shape for Case 2

Figure 2-5. Optimized shape for Case 2

Table 2-2. Results for Initial and Optimized Shape of Case 2

Parameter	Initial Shape	Optimized Shape
Objective Function (*m*)	1000000	4.480×10^{-3}
Mass of the Assembly (*kg*)	1662.48	1894.35
Maximum Z-coordinate (*m*)	0.0214	0.1376
Minimum Z-coordinate (*m*)	0.0167	-0.0999
Maximum Plastic Strain	0.23909	0.02078
Minimum thickness (*m*)	0.0047	0.0236

Case 3: Initial Shape Violating Mass, Envelope and Minimum Thickness Constraints

To violate even more constraints simultaneously a non-flat initial shape was devised such that the thickness of the edges of the plate violates the envelope constraints, the mass of the assembly exceeds the mass constraint, and concavities on the front- and back-faces in the middle of the plate reduce the thickness of the plate below the minimum allowed thickness (see Fig. 2-6). The violations were again corrected by the optimizer (see Fig. 2-7). The results are reported in Table 2-3.

Figure 2-6. Initial shape for Case 3

Figure 2-7. Optimized shape for Case 3

Table 2-3. Results for Initial and Optimized Shape of Case 3

Parameter	Initial Shape	Optimized Shape
Objective Function (*m*)	1000000	4.849×10^{-3}
Mass of the Assembly (*kg*)	5096.59	1893.31
Maximum Z-coordinate (*m*)	0.3168	0.13996
Minimum Z-coordinate (*m*)	-0.2787	-0.09998
Maximum Plastic Strain	0.00029	0.01876
Minimum thickness (*m*)	0.0041	0.0258

The stiffener, though present, is not shown in any of the images for clarity. The higher value of the objective function for the initial shapes is due to the penalty for constraint violation. In all three cases all of the constraint violations are corrected, and the shape optimization results in exactly the same double-bulged shape.

2.3 Investigation of Effect of Boundary Conditions on Panel Response and Optimized Shape

For all the optimization cases discussed previously a free plate has been used. To study the effect of boundary conditions, other boundary conditions were also investigated as follows.

Three identical flat solid isotropic aluminum plates with three different sets of boundary conditions were subjected to identical air blasts. In each case the front-face of the plate faces the blast. The plates with the boundary conditions are shown in Figures 2-8 – 2-10.

In the first case the nodes along the bottom edges of the plate were pinned, i.e., the translational degrees of freedom of these nodes were constrained. This would be analogous to a pinned-pinned condition as the plate is free to rotate about these nodes, i.e., only reaction forces, no reaction moments are produced at these boundaries.

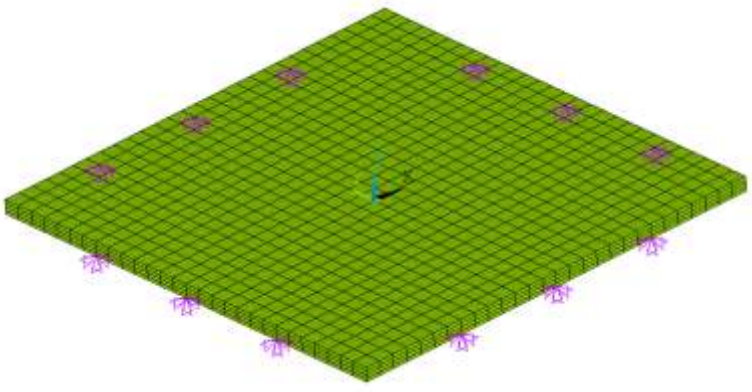

Figure 2-8. Case 1: Plate with sides pinned

For the second case the translational degrees of freedom of all the nodes along the sides of the plate are constrained. This corresponds to the fixed-fixed ends. Both reaction forces and reaction moments result from this boundary condition.

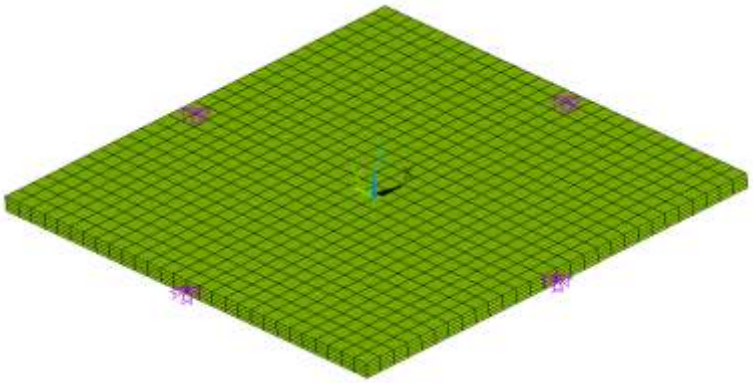

Figure 2-9. Case 2: Plate with sides fixed

In the third case the plate was enclosed by a free grip system used by Argod, et al. in [6]. This grip system, akin to stiffener used in previous optimization cases, provides additional stiffness and inertia to the plate while also avoiding plastic strain concentrations around the edges and corners.

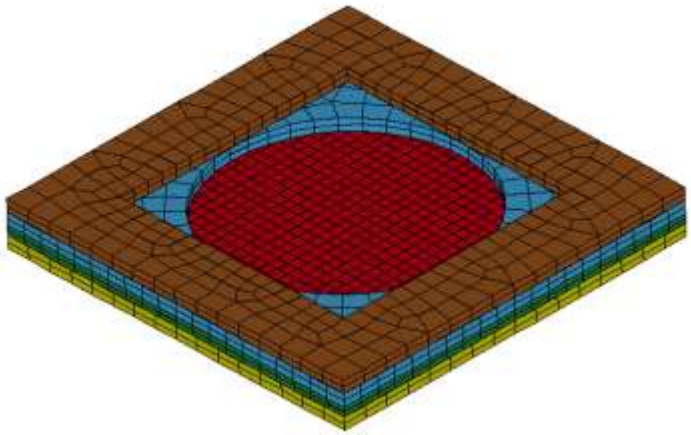

Figure 2-10. Case 3: Plate with a freely supported grip assembly

The displacement versus time response of the flat (baseline) shapes to a central charge was qualitatively the same (see Fig. 2-11). Maximum plastic strain magnitudes (see Fig. 2-12) are only slightly different while distributions (i.e., locations) (see Fig. 2-13) of maximum plastic strain are significantly different. The numerical results are recorded in Table 2-4.

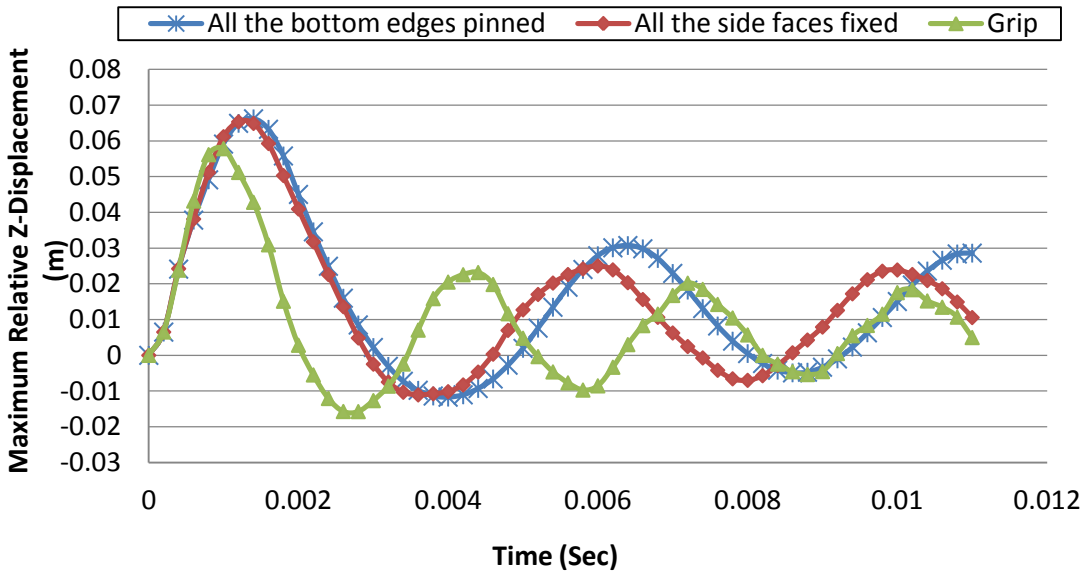

Figure 2-11. Maximum relative-Z displacement

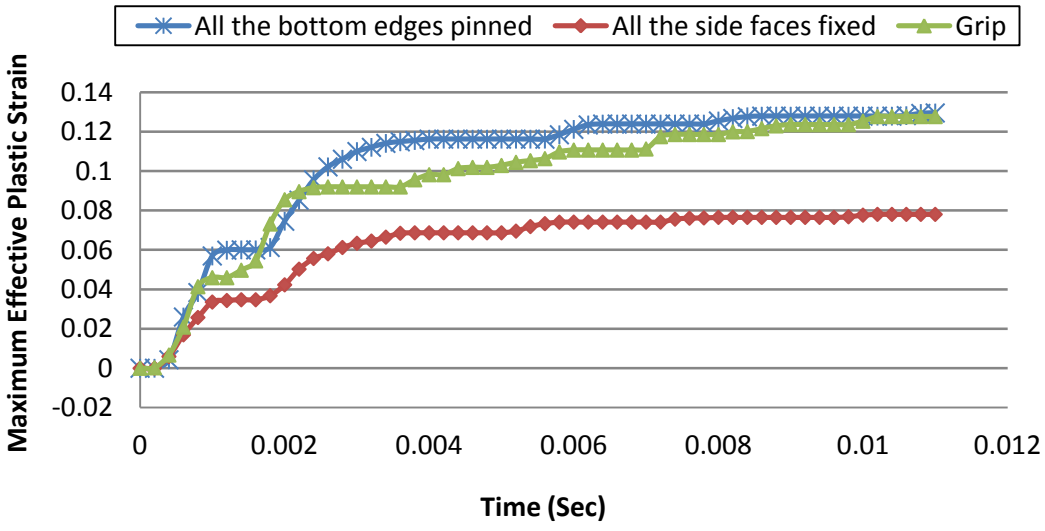

Figure 2-12. Maximum effective plastic strain

Table 2-4. Comparison of Performance of Baseline Plate for Different Boundary Conditions

Parameter	Case 1	Case 2	Case 3
Objective function of baseline shape (m)	29.83×10^{-03}	27.69×10^{-03}	20.51×10^{-03}
Maximum Relative Z-Displacement (*m*) (at first peak)	0.0662	0.0653	0.0578
Maximum Effective Plastic Strain	0.130	0.078	0.128
Mass of baseline shape (kg)	152.913	152.913	152.913[1]

[1] Mass of the plate of interest only

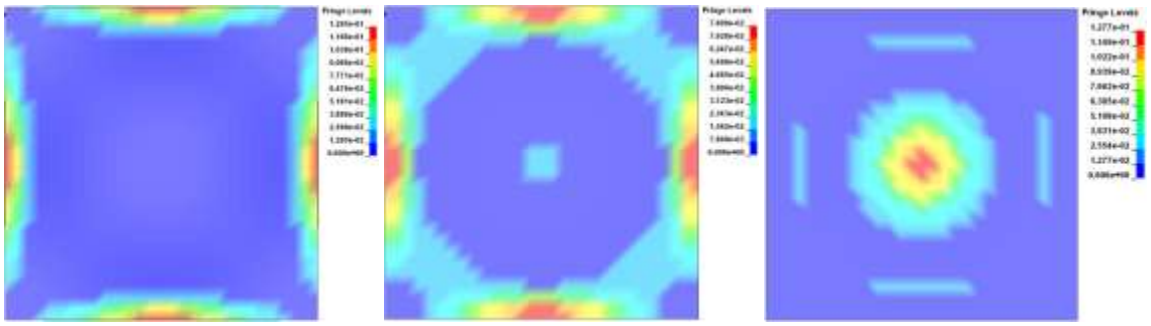

Case 1: Front-face Case 2: Front-face Case 3: Back-face

Figure 2-13. Distribution of effective plastic strain on the face where it is maximum

The fixed-fixed boundary condition (Case 2) being marginally more restrictive than the pinned-pinned boundary condition (Case 1) gives slightly less relative displacement while distributing the plastic strain more effectively, consequently producing significantly lower maximum plastic strain. The grip system being free produces the smallest relative displacement as all parts of the plate move in response to the blast, albeit differently. The grip system concentrates the plastic strain at the center of the plate by supporting and partially shielding the extremities of the plate.

Further, shape optimization of the three baseline designs was performed using three design variables (3-DV). The optimized shapes are shown in Figures 2-14 – 2-16, and the results are presented in Table 2-5.

Figure 2-14. Case 1: Optimized shape for plate with sides pinned

Figure 2-15. Case 2: Optimized shape for plate with sides fixed

Figure 2-16. Case 3: Optimized shape for plate with a freely supported grip assembly (not shown)

Table 2-5. Comparison of Performance of Plates Optimized for Different Boundary Conditions

Parameter	Case 1	Case 2	Case 3
Objective function of optimized shape (m)	13.14×10^{-03}	10.36×10^{-03}	4.49×10^{-03}
Maximum Relative Z-Displacement (*m*) (at first peak)	0.0217	0.0176	0.0077
Maximum Effective Plastic Strain	0.05105	0.03703	0.02028
Maximum Z-coordinate (*m*)	0.0720	0.0784	0.1376
Minimum Z-coordinate (*m*)	-0.0889	-0.0886	-0.0999
Minimum thickness (*m*)	0.0413	0.0405	0.0236
Mass of optimized shape (kg)	220.428	220.349	207.723[1]

[1] Mass of the plate of interest only

Shape optimization of the baseline design with different boundary conditions yields qualitatively the same shape, namely a double bulge. The thickness of the plate of interest outside the domain of shape optimization is less in Case 3 (grip assembly) as compared to the other two cases. In Cases 1 and 2 the ends of the plate are constrained; therefore, to reduce the deflection, the plate has to be thicker to be stiffer. In Case 3 the plate is freely supported, and additional stiffness is provided by the grip assembly. The extent of the bottom bulge is similar in all three cases as it plays an important role in deflecting the blast waves. Since the constraint on mass is the same in all three cases, the first two cases have smaller top bulges to compensate for increased thickness of the plate.

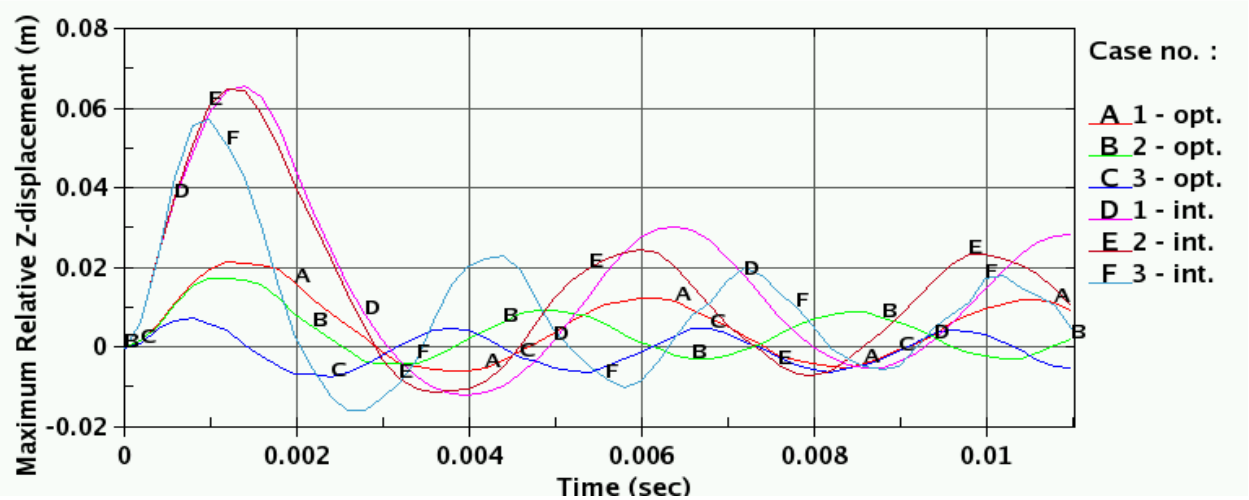

Figure 2-17. Maximum relative Z-displacement of optimized (3-DV) and baseline shapes

From Fig. 2-17 we can see that even after optimization the displacement curves still retain the dynamic signatures of their initial shapes. The displacement for the plate with fixed sides is slightly less than that of the pinned one. As we progress from pinned to fixed plate to grip system we see shortening ‘cycles’ both in the baseline and the optimized shapes. Thus, being subjected to blast load is unlike high speed impact problems where boundary conditions would not be critical to the optimized shape.

2.4 Convergence of Shape With Regard to Increasing Number of Velocity Fields

The optimization problem described earlier was solved using increasing number of design variables, i.e., with 3, 5, 7, 9 and 11 velocity fields. The 5-DV case consists of the basis shapes used in the 3-DV case along with additional shapes, and so on analogous to any series expansion. The 3-DV case corresponds to deformations due to loads at the center-point on front and back surfaces, respectively, along with a thickness change. The 5-DV case includes the velocity fields from the 3-DV case along with two more deformations due to loads at the quarter-point on front and back surfaces, respectively. Similarly, the 7, 9 and 11 DV cases are obtained by adding velocity fields at the remaining quarter-points on both front and back surfaces. Note that the 3-DV case can produce only a symmetric shape since each velocity field is symmetric. For the purpose of comparison a baseline design (flat plate with stiffener) of the same mass as the optimized shapes has been included in the study.

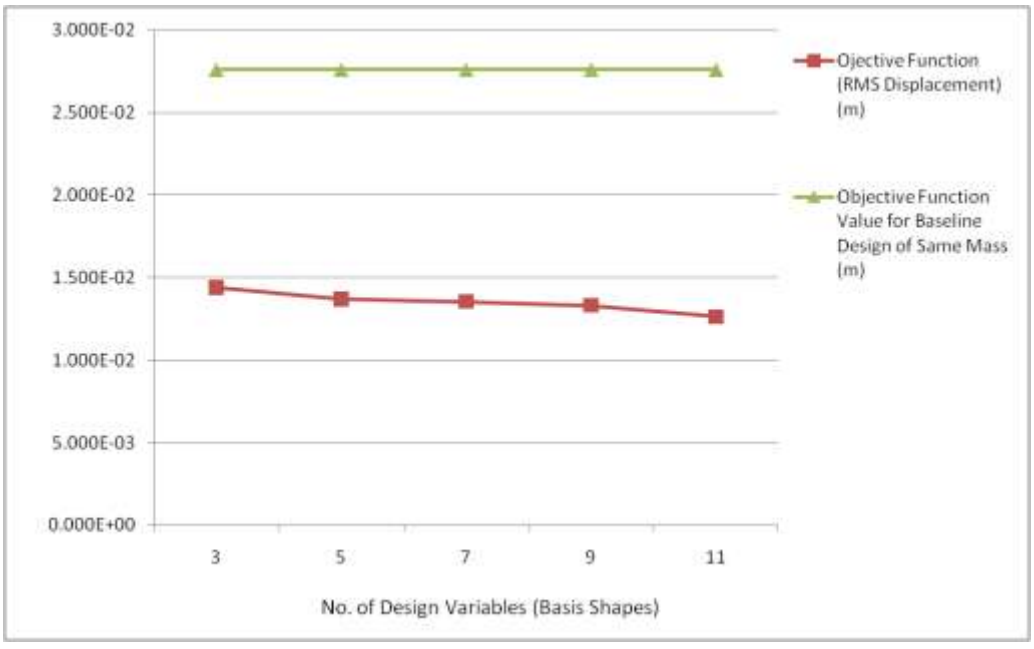

Figure 2-18. Objective function values for shapes with different number design variables

Table 2-6. Objective Function and Maximum Effective Plastic Strain Values for Different DV Cases

Case	Objective Function (m)	Maximum Eff. Plastic Strain
Baseline Design	2.760E-02	0.04629
3-DV	1.440E-02	0.01752
5-DV	1.372E-02	0.02279
7-DV	1.355E-02	0.02333
9-DV	1.332E-02	0.02841
11-DV	1.264E-02	0.02530

Results show that moderate convergence of the objective function is obtained (see Fig. 2-18 and Table 2-6) and that plastic strain is smeared on the front surface in all the cases. The plastic strain constraint is not active in any case while the mass constraint is active in all cases. Regarding shape, a bottom bulge is obtained in all the cases. The bulge is symmetric in shape with the maximum bulge being located approximately at the center of the plate. However, there are small variations in the shape of the top bulge in each case. This indicates that a study with larger number of variables needs to be undertaken which will require development of improved optimizers.

2.5 Optimization of All-Metal Plate for Off-Center Charge Locations

The optimization of the all-metal plate with a grip system was carried out in four ‘steps’, each successively offsetting the charge by a distance of $L/24$ (L being the length of the plate of interest) along the x-axis from the initial center position. The y and z coordinates remained the same at 0 and -0.4064 m, respectively. The double-bulged plate obtained through optimization for

center charge location was used as the initial shape for optimization at the first offset charge location. In each subsequent step the previous step's optimized shape was used as the initial shape. 11 and 7 basis shapes (velocity fields) were used, respectively, for unsymmetric and symmetric shape variations. The evolution of the shape of the plate as a result of charge offset is shown in Fig. 2-19.

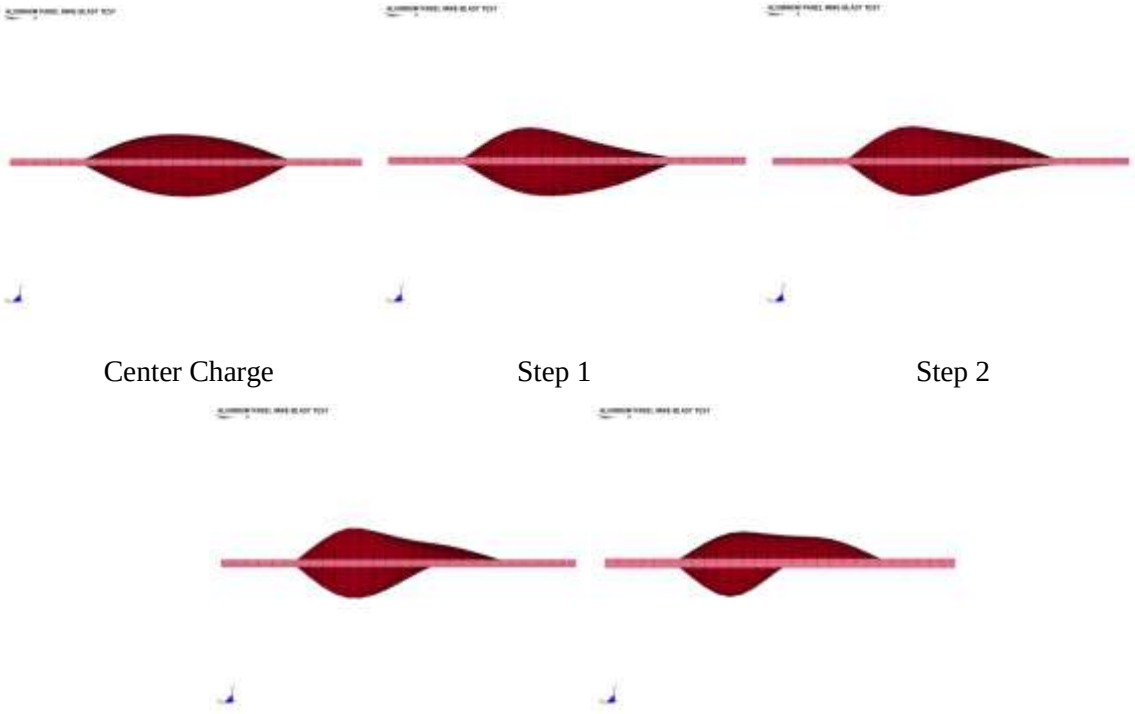

Figure 2-19. Right profile view of the optimized plates with increasing charge offset (towards the left, in steps of $L/24$ from center, L = length of 'plate of interest')

Step 3 onwards a cavity appeared on the front-face of the plate over the –X-axis (see Fig. 2-20).

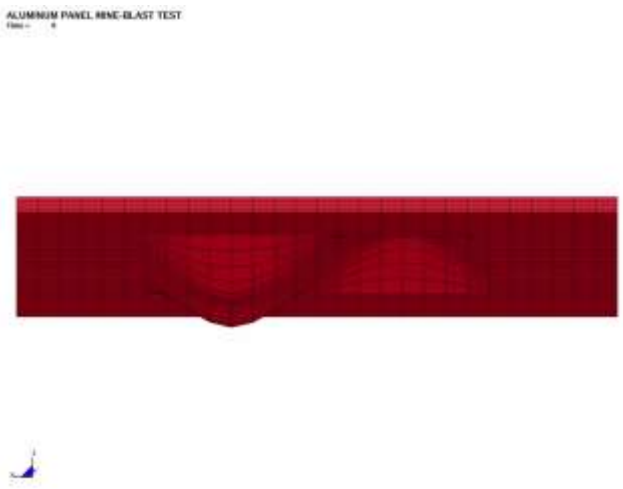

Figure 2-20. Cavity on the front-face of the plate (Step 4)

As the charge is offset along the X-axis, the bottom bulge migrates with it in order to deflect the blast waves. The thickness (bulge) of the plate increases until the mass limit is reached. Thereafter a cavity is formed to get more mass above the charge location. The C.G. of the plate shifts in the direction of the off-center charge. Figure 2-20 shows this cavity in detail. Table 2-7 contains the response values.

Table 2-7. Optimization Results for Off-Center Charge Locations

Charge Location	RMS Relative Displacement (m)	Max. Relative Displacement (m)[1]	Max. Plastic Strain	Total Mass of the assembly (kg)
Center	4.4806E-03	7.3971E-03	0.0231	1894.54
Step 1 (L/24)	4.6171E-03	9.1604E-03	0.0367	1895.52
Step 2 (L/12)	4.8339E-03	1.0882E-02	0.0361	1891.77
Step 3 (L/8)	4.9089E-03	1.2581E-02	0.0293	1894.25
Step 4 (L/6)	5.1523E-03	1.4533E-02	0.0440	1893.00

[1]Relative Displacement = δ_{domain}-$\delta_{fixture}$ (occurs at 1st peak)

Verification Study of Optimality for Off-center Charges

Owing to the difficulty in using the stochastic optimizer on this problem, a coarse verification of optimality was carried out by shifting the charge a step backward (along X-axis) and a step forward for each step. It was verified that the shape obtained for each step was best for the charge location for which it was optimized. Another way of interpreting the results is that for a given charge position the shape optimized for it is better than either of the adjacent step shapes. A chart of the verification results is provided below in Figure 2-21.

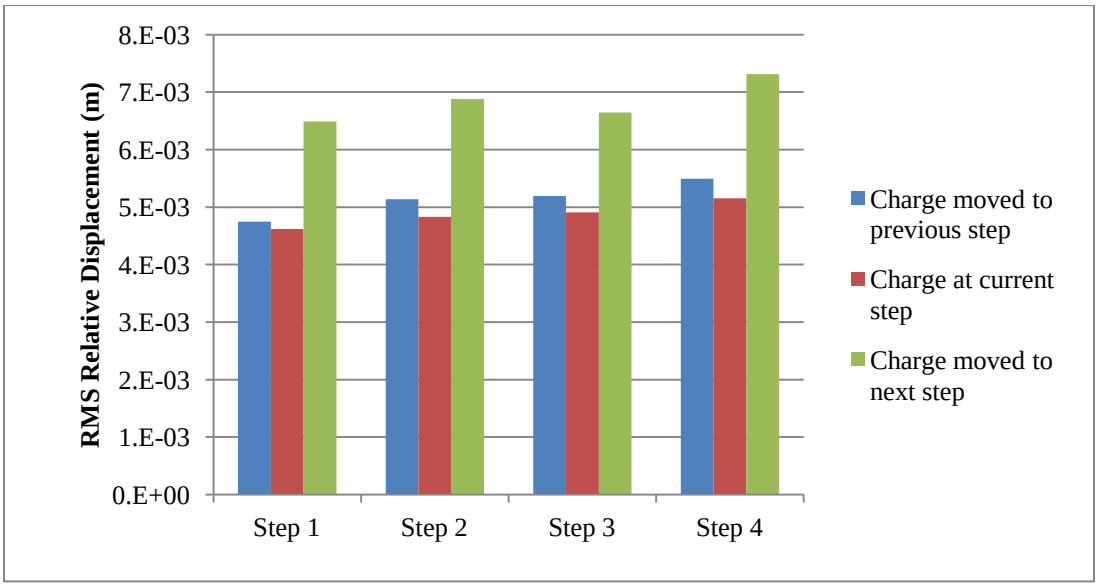

Figure 2-21. Verification study of optimality for offset charges

2.5 Summary and Conclusions

Various feasible and infeasible shapes were optimized to reach the same convex-double bulged shape. This independence from the starting point of the optimization proves that the problem formulation is well-posed. This numerical experiment also displays the robustness of the stochastic optimizer (DE).

Next, panels with different boundary conditions, viz. fixed sides, pinned sides and freely suspended grip system were optimized to study their effect on the solution. Significant differences were seen in the displacement response as well as the distribution of plastic strain. Insight was also gained into how the optimizer allocates the available resource, namely mass, in order to achieve minimum deflection. The bottom bulge was found to be vital as it deflects the blast waves. So the optimizer maximized the bottom bulge for all the cases. Boundary conditions that provided stiffness to the structure allowed more mass to be added to the top bulge, stiffening the center of the plate as well as providing inertia. This study also established that blast is unlike a ballistic impact problem where boundary conditions are less critical to the optimized design. The freely suspended grip system was adopted and later modified for all subsequent optimizations.

It was shown that the number of design variables (velocity fields) used in the optimization studies were adequate to capture the optimum shape. Moderate convergence in the objective function value was obtained with increasing number of velocity fields. A bottom bulge was obtained in all the cases showing that it is essential to reduce deflection. However, there were small variations in the top bulge indicating that a study with larger number of variables needs to be undertaken. This depends on the development of improved optimizers, specifically response based methodology, and availability of larger computational resources.

Optimized shapes were obtained for off-center charge locations and verified. The bottom bulge migrated in the direction of the charge offset, trying to position itself directly over the charge in order to deflect the blast waves effectively. The top bulge also leaned toward the offset charge shifting the center of gravity of the panel in the direction of the off-center charge.

Chapter 3

Validation of Homogenized Honeycomb Stress-Strain Curve

A stress-strain curve for a honeycomb core with face plates based on uniaxial crushing has been generated by Sumanta [11]. However, this stress-strain curve is being used in a plate that undergoes bending as well. The question that arises is: how good is the homogenized stress-strain curve in this more general load environment? This is investigated in this chapter where deflections, stiffness and energy absorption are compared between a finite element (FE) model based on the homogenized stress-strain curve and a detailed FE model of the honeycomb sandwich.

3.1 Large Scale Uniaxial Crush Test of a Detailed Finite Element Model

For optimization, the honeycomb core was modeled as a continuum solid structure with equivalent mechanical properties of the actual core. The equivalent mechanical properties were determined by virtual testing method and parameterized in terms of the important honeycomb cell parameters [11]. The main steps in obtaining the parameterized mechanical properties were: (1) a unit cell was identified, and a FE model of this cell was developed (see Fig. 3-1); (2) geometrical parameters associated with the unit cell were identified; (3) nonlinear virtual testing was carried out for different values of the geometrical parameters, followed by curve fitting (see Fig. 3-2) which parameterized the stress-strain curve in terms of the geometrical parameters; (4) the homogenized model was validated by comparison to existing results in the literature. The unit cell was used for this parameterization to save computational time for repeated virtual crush tests.

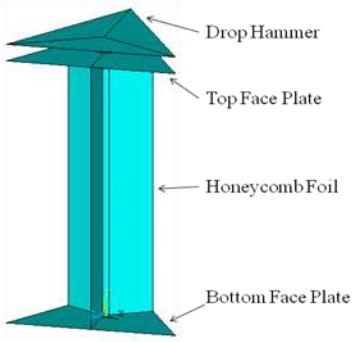

Figure 3-1 Unit cell used for uniaxlial crush test

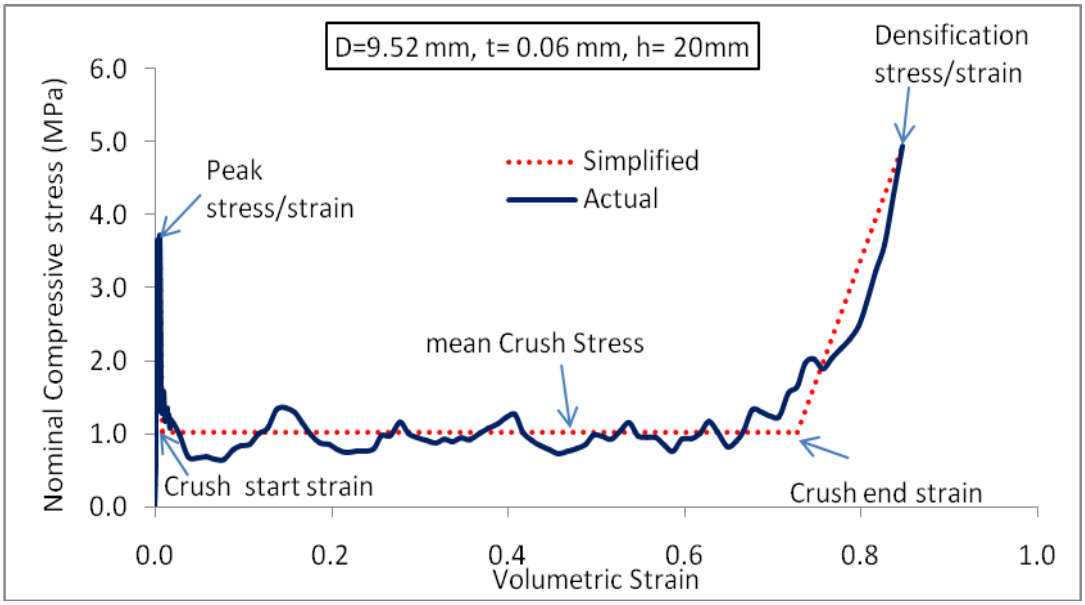

Figure 3-2 Load curve obtained by unit cell crushing, its simplified fit and different parameters

To validate that the stress-strain curve obtained here is good enough to approximate the behavior of a larger cluster (honeycomb) of unit cells, where the unit cells interact with one another instead of being constrained by symmetry boundary conditions, a detailed FE model of a test specimen (see Fig. 3-3) is crushed. The stress-strain obtained by this large scale crush test is then compared to the parameterized curve for the equivalent unit cell [11] (Fig. 3-4). A reasonably good match between the two curves establishes that the homogenized curve adequately represents the honeycomb material in uniaxial crushing.

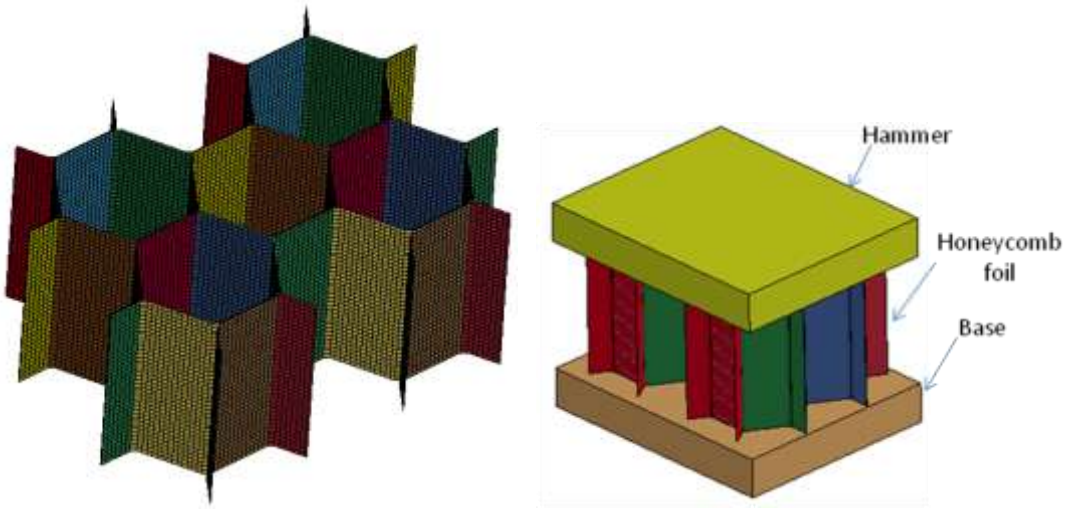

(a) (b)

Figure 3-3 (a) Detailed large scale finite element model of the core (b) Test setup for uniaxial crushing of the detailed model

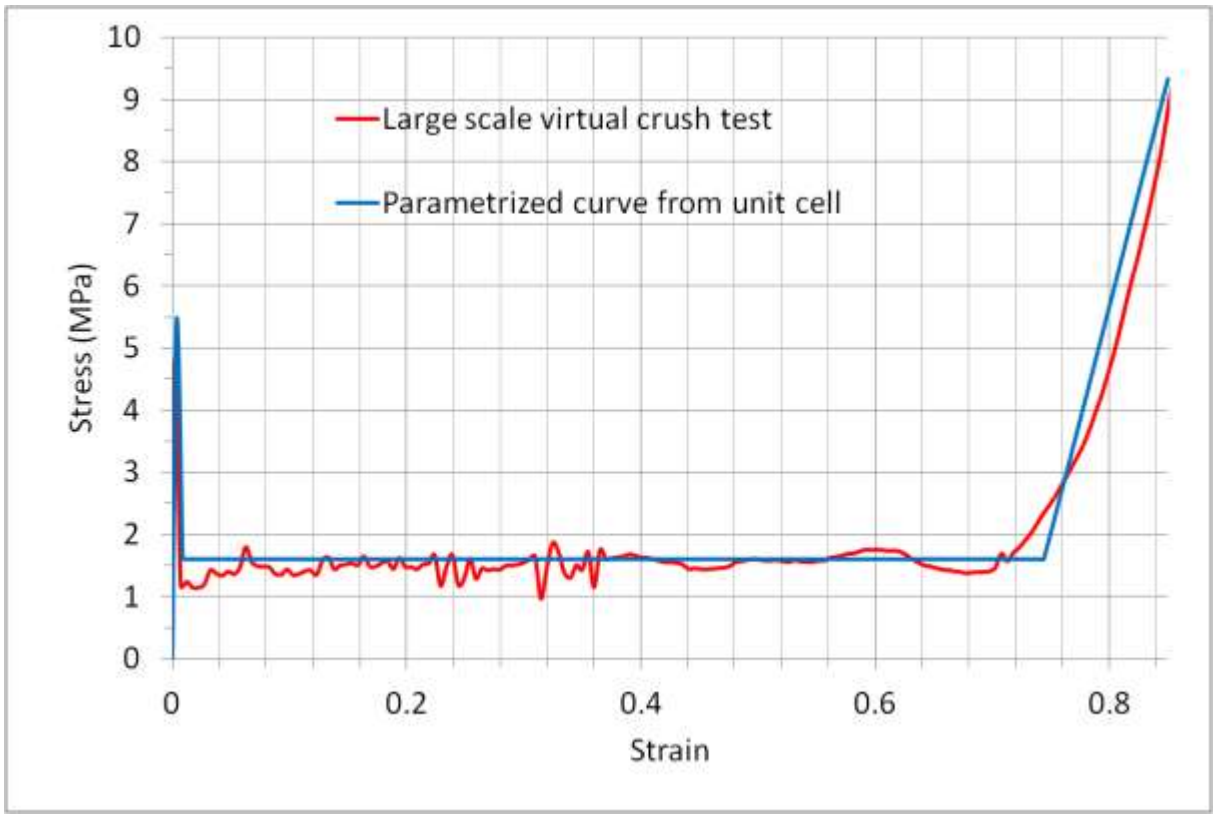

Figure 3-4 Comparison of stress-strain curve obtained by crushing the detailed model with the parameterized curve from the unit cell crush test [11]

3.2 Validation of Honeycomb Model through Flexure Tests

When the honeycomb sandwich is subjected to blast loading it not only undergoes axial crushing but also flexure. Virtual flexure tests are performed and comparisons are made in accordance with the provisions of ASTM standards D 7250 [12] and C 393 [13] in order to gauge the accuracy with which the homogenized model can replicate the response of the detailed model in flexure. The practices include cores with discontinuous bonding surfaces like honeycombs. The sandwich is subjected to flexure in a manner so as to produce curvature in the facing plates.

The testing is done with the ribbon of the honeycomb core both parallel and perpendicular to the span to exclude any interference from core orthotropy. As the modulus of the sandwich facings is known and the facings are identical a single loading configuration test is required [23]. As per the standard practice C 393 [24] the standard 3-point (midspan) loading configuration is used.

To reduce computational time while modeling enough elements along the depth to capture crushing and along the span to capture flexure accurately, symmetry in the geometry and loading configuration is exploited. In order to include complete cells within the models with both orientations of the ribbon the geometrical dimensions the detailed models and their homogenized equivalents are slightly different as shown in Table 3-1.

Model Specification

Geometry

Table 3-1. Dimensions of the Models

Dimensions	Ribbon parallel to span	Ribbon perpendicular to span
Length (mm)	132	130.737
Breadth (mm)	28.989	33
Core Thickness (mm)	12.7	12.7
Face Plate Thickness (mm)	0.813	0.813
Span Length (mm)	82.5	82.8
t/D	0.007535 (0.0724/9.608)	0.007535 (0.0724/9.608)
Adhesive Thickness (mm)	0.082	0.082

Ribbon parallel to the span

Owing to the symmetry about the midspan only half the span is modeled (see Fig. 3-5). Symmetry boundary conditions are applied on the nodes at the midspan, belonging to both the sandwich and the loading block.

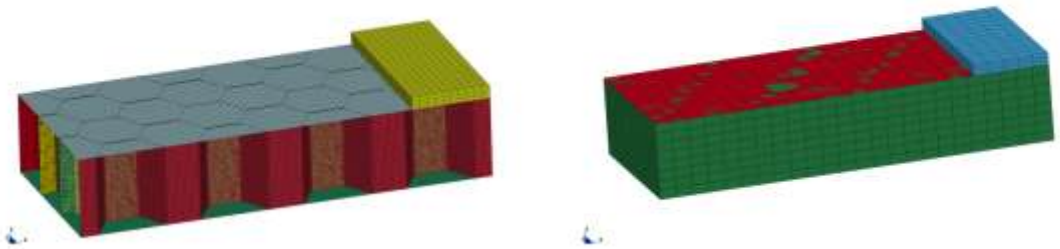

(a) Detailed Model (b) Homogenized Model

Figure 3-5. Honeycomb ribbon orientation parallel to span of sandwich beam

Ribbon perpendicular to the span

In this case the full span of the sandwich beam is modeled but only with half the width (see Fig. 3-6). Accordingly half the width of the loading block is also modeled. Symmetry boundary conditions are applied on the nodes on the symmetry face.

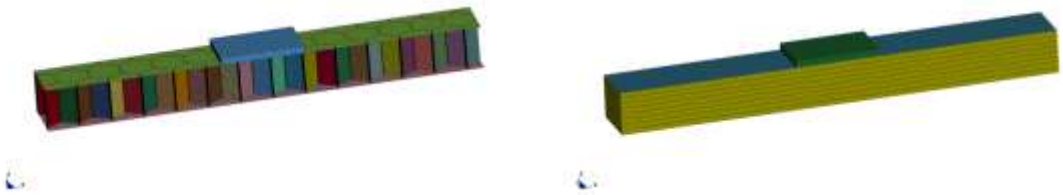

(a) Detailed Model (b) Homogenized Model

Figure 3-6. Honeycomb ribbon orientation perpendicular to span of sandwich beam

Supports and Loading

The sandwich beam is supported by fixing the translational degrees of freedom of the nodes on a line on the bottom facing plate perpendicular to the span. The applied load is distributed over an area through a block with Young's modulus, yield stress and tangent modulus $1/10^{th}$ of those for aluminum to simulate a soft loading block. The length of the block is 25 mm, height 2 mm, and width equal to the width of the sandwich. The nodes on the top face of the block have a prescribed motion of 127.5 mm in 0.1 seconds. The simulation time is 0.01 seconds so that the actual motion is 12.75 mm. The loading block is in contact with the top face plate at the beginning of the simulation. This allows free rotation of the beam at both the support and loading points. The nodes at the top and bottom faces of the core are tied to the top and bottom face plates respectively to simulate bonding.

Material

The material properties of the ribbon foil and the adhesive used in the core of the detailed FE model are provided in Table 3-2. For the homogenized version the core is replaced by a homogeneous block of the exact same dimensions as the core and the equivalent homogenized material properties (see Table 3-3) using the *MAT_CRUSHABLE_FOAM keycard and the stress-strain curve in LS-DYNA. The face plates have the same material properties as the foil.

Table 3-2. Material Properties of Components of the Detailed Honeycomb

Material	Density (Kg/ m^3)	Young's Modulus (GPa)	Yield Stress (MPa)	Tangent Modulus (MPa)	Poison's Ratio
Foil-Al5052	2680	72	300	50	0.34
Adhesive	2000	5	30	0	0.3
Loading Block	3000	7.2	30	5	0.34

Table 3-3. Material Properties of Homogenized Equivalent

Material	Density (Kg/ m^3)	Young's Modulus (GPa)	Poison's Ratio	Tensile Stress Cut-off (MPa)	Crush Stress (MPa)
Homogenized Core (t/D = 0.007535)	53.85	1.363	0.00	6.028	1.5771

3.3 Results

The total force applied on the top of the loading block and the displacement of a node at the midspan at exactly half the thickness of the core is measured. The ASTM standard D 7250 [12] prohibits the calculation of stiffness properties at any force level above or beyond the point of initial failure – seen here as core crushing – or above a point where the specimen exhibits obvious non-linear force-deflection response due to excessive local or overall deflection. However, as the objective is not to determine these stiffness properties but merely to compare the behavior of the detailed and the homogenized models, more importantly while they are being crushed in flexure, we load the beam beyond the initiation of core crushing.

Deflection Response

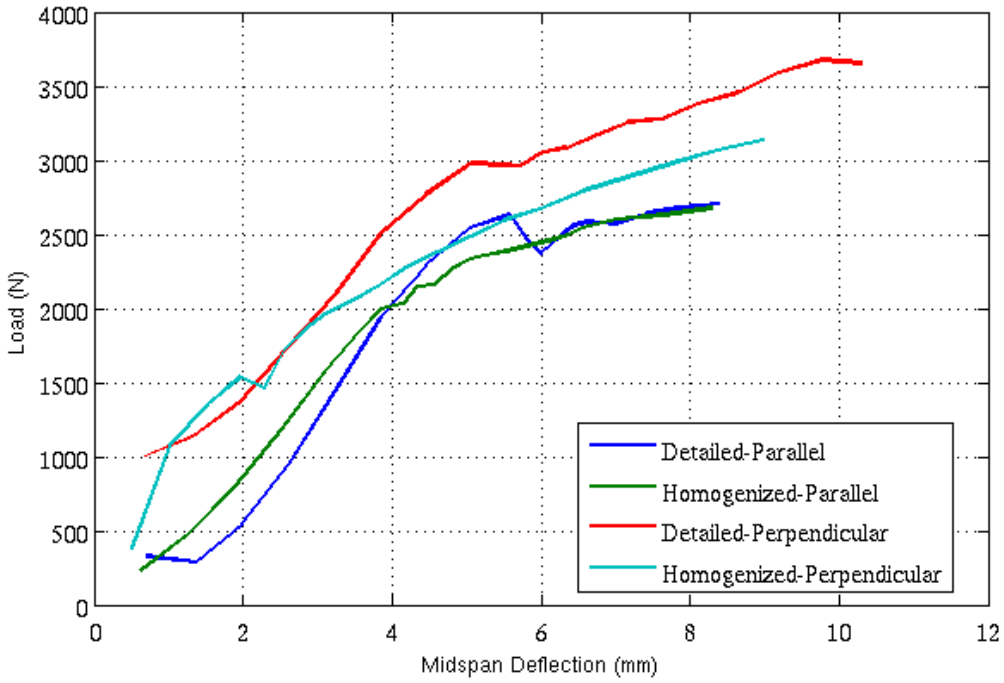

Figure 3-7. Load vs. midspan deflection

From Fig. 3-7 we can see that the general nature of the deflection response for all the models is similar. The unavoidable differences in the size of the parallel ribbon and perpendicular ribbon models account for the slightly higher load required to deflect the latter.

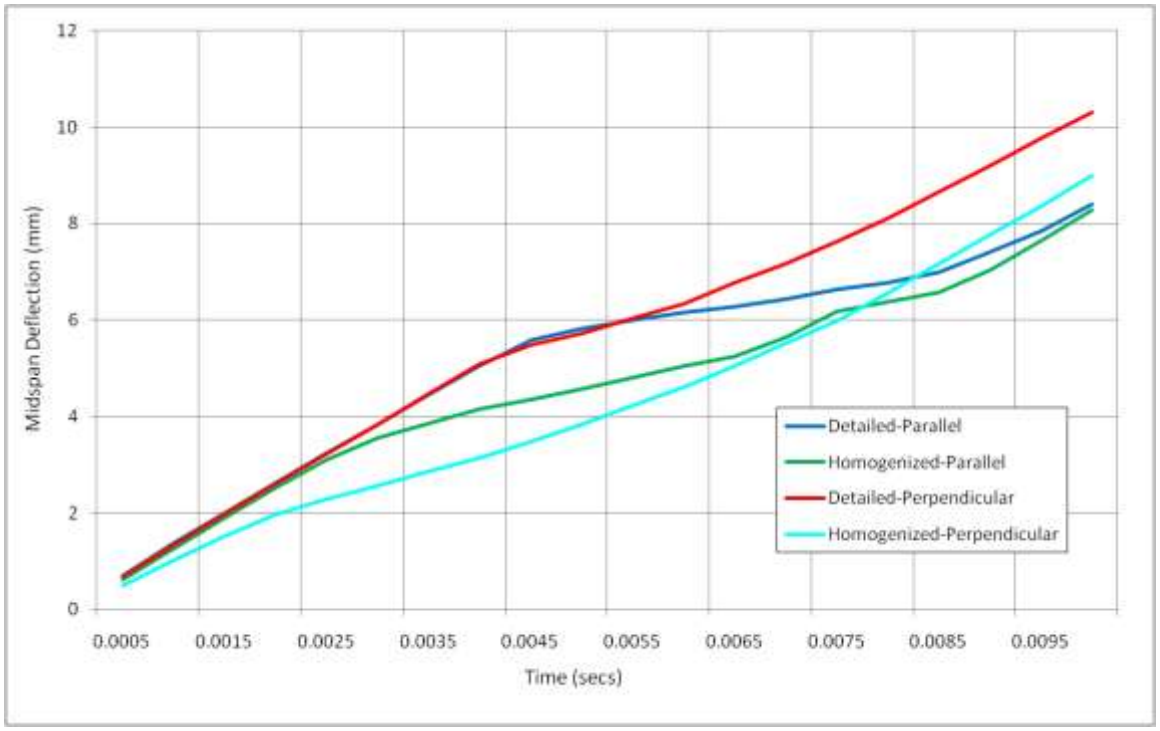

Figure 3-8. Midspan deflection vs. time

In Fig. 3-8 we see that there is a marked zone of transition in the response of the detailed models around 4.5 milliseconds. The slope is constant up to this point and then changes. In the detailed model crushing begins locally, and as the load increases further the crushed zone expands further. The transition marks the beginning of crushing in the midspan plane. On the other hand, in the homogenized model the equivalent foam core compresses uniformly throughout the thickness. Once crushing has commenced in the detailed model, the deflection

increases faster, reaching values similar to the homogenized model once the core under the loading block has been significantly crushed.

Calculation of Stiffness Values

The transverse shear rigidity and core shear modulus are calculated as per the standard practice D 7250 [12] and plotted with respect to time (corresponding to different force values) in Figs. 3-9 and 3-10. We can see that there is good agreement in the values especially after crushing has commenced in the detailed models. The transverse shear rigidity and core shear modulus values are within ±5% of each other.

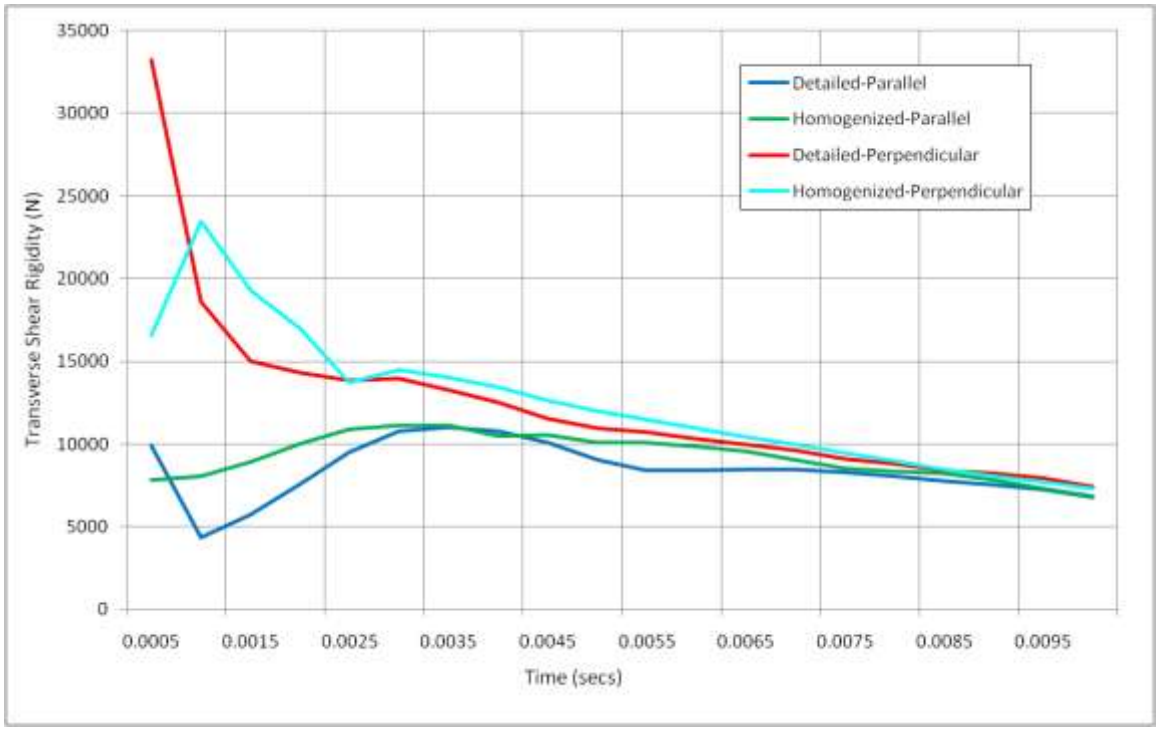

Figure 3-9. Transverse shear rigidity

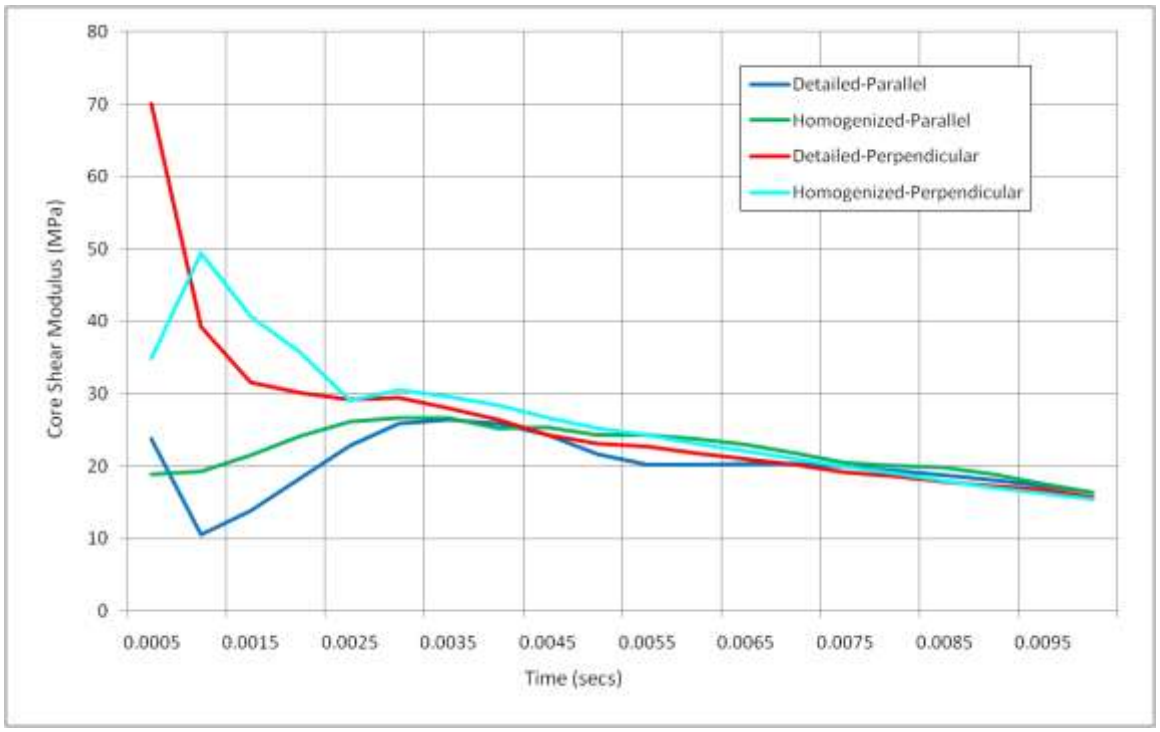

Figure 3-10. Core shear modulus

Comparison of Captured Energy

Due to the low mass of the models combined with the low velocity acquired over the simulation, the kinetic energy is negligible compared to the internal energy gained for each of them.

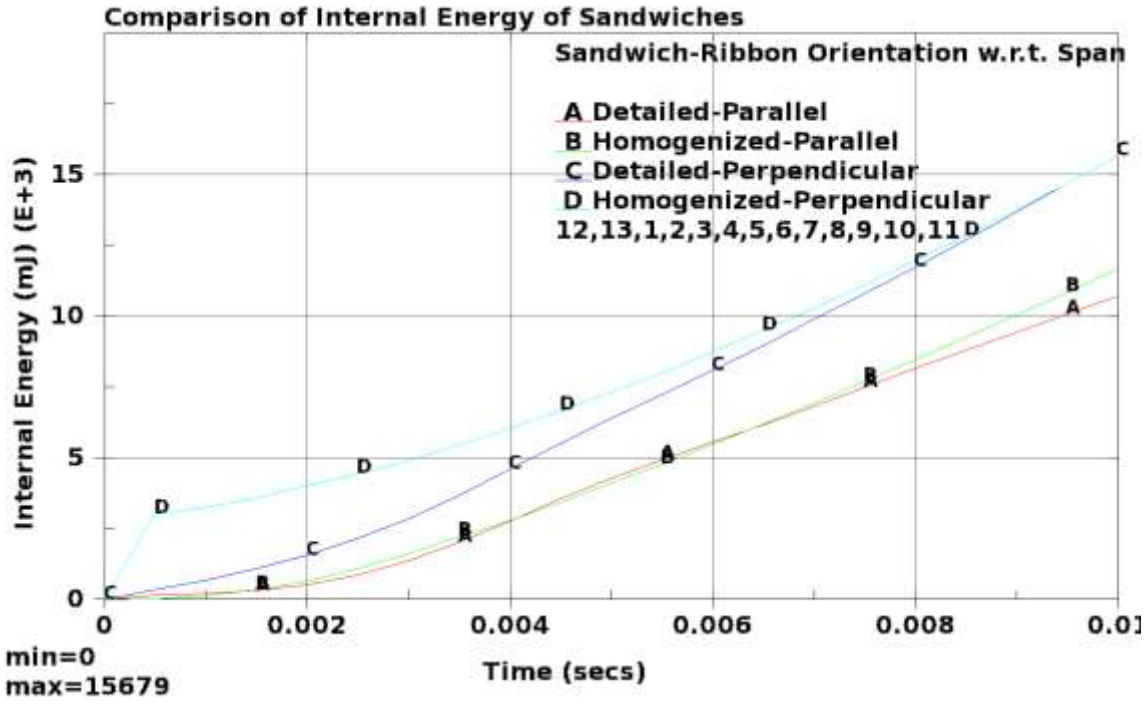

Figure 3-11. Comparison of internal energy captured by the sandwiches

Due to difference in the size of the parallel-ribbon and perpendicular ribbon models the energy captured by them is different. Even so the energy captured by the detailed model agrees very well with homogenized model for each orientation (±5%).

3.4 Code Modifications to Handle Honeycomb Material Properties as Design Variables

The FORTRAN optimization program was modified in order to be able to handle the honeycomb material properties as design variables. The parameterization of honeycomb material's stress-strain curve in terms of the ratio of its foil thickness (t) to the cell size (D) [11] is utilized here. The t/D ratio was used as the sizing design variable for honeycomb material in the design input file. Appropriate limits based on commercial fabrication practices for honeycomb [9] were used. Modifications were made to the program subroutines to read the new input file and

process the parameter to be used as a variable in DE in addition to the shape design variables. A subroutine was added to calculate the new material properties for each new member of the design population and write them in the appropriate keycard format to the LS-DYNA input file. Other aspects and parameters pertaining to DE were same as discussed in Section 2.1.

3.5 Summary and Conclusions

A large scale uniaxial crush test is performed to validate that the parameterized stress-strain curve obtained from the uniaxial crushing of a unit cell [11] adequately represents the behavior of the actual honeycomb. From Fig. 3-2 and 3-4 we can see that the parameterized curve gives as good a fit to the stress-strain curve obtained from large-scale crush test as it gives to the one obtained from crushing the unit cell. This gives us confidence that the parameterization performed in [11] can be used for homogenizing the model for uniaxial crushing.

As the honeycomb core undergoes flexure during application of the blast load we perform 3-bending tests on a honeycomb core sandwich and compare it with its homogenized equivalent. Since the honeycomb is orthotropic, bending tests are performed with honeycomb ribbon orientation both parallel and perpendicular to the span of the beam. Differences are seen in the crushing behavior as the detailed honeycomb core provides greater stiffness before it begins crushing locally. The homogenized core on the other hand crushes uniformly throughout. These differences dissipate as the crushing progresses. Similar trends are seen in the graphs of transverse shear rigidity and core shear modulus. The energy captured by the honeycomb sandwich in bending is also compared. The calculated stiffness values and the energy captured by the honeycomb core sandwich match within 5% with the homogenized equivalent irrespective of the orientation of the honeycomb ribbon with respect to the span. It is interesting that a homogenized model based on uniaxial crushing only captures behavior in beam bending in two

directions. So we can replace the detailed core with its homogenized equivalent for subsequent simulations and for optimization. Replacing the detailed core with the homogenized equivalent not only enables the simulation of models with more complicated geometry and loading where the detailed core would have failed to converge but also saves significant computation time. Where the bending of the detailed model took ≈ 48 hours on a single processor, the simulation of the equivalent homogenized core only took 18 mins.

Modifications were made to the FORTRAN code so that it could handle honeycomb material properties as design variables for the DE optimizer. This paves the way for simultaneous shape, size and core optimization for honeycomb sandwich panel.

Chapter 4

Conclusions

The optimization problem for the all-metal plate is found to be well-posed. Different initial shapes converge to the same optimized double-bulged shape. Even starting shapes that violate the constraints are optimized to the double-bulged shape. The DE algorithm shows its robustness. The all-metal plate is optimized with different boundary conditions, all resulting in qualitatively the same shape, namely a double bulge. The extent of the bottom bulge is the same in all cases as it plays an important role in deflecting the blast wave. Boundary conditions that provide stiffness to the plate allow for thinner, less stiff plates to have the same deflection as thicker plates with boundary conditions that do not provide edge stiffness; the mass that now becomes available on account of the plates being thinner is utilized by the optimizer to increase the size of the top bulge. This, in turn, leads to these plates having less relative displacement of the back-face. The optimizer shows moderate convergence of the objective function with increasing number of design variables. A study with larger number of variables needs to be undertaken that will require development of improved optimizers, specifically response surface methods.

In the offset-charge study we find that as the charge is offset along the X-axis the bottom bulge migrates with it in order to deflect the blast waves. The bulge of the plate increases until the mass limit is reached. Thereafter a cavity is formed to get more mass above the charge location. The center of gravity of the plate shifts in the direction of the off-center charge.

The stress-strain curve obtained by crushing the large scale detailed finite element of the honeycomb fits well with the parameterized curve obtained from the unit cell crush test. This shows that the parameterized curve can accurately represent the honeycomb sandwich core in crushing. Three-point bending test is performed on the detailed honeycomb finite element model

for both ribbon orientations perpendicular and parallel to the span. The equivalent homogenized model is subjected to the same loads. The deflection response, stiffness values and energy captured by sandwich in flexure are compared for both. We see that the calculated stiffness values and the energy captured by the honeycomb core sandwich match within 5% with the homogenized version irrespective of the orientation of the honeycomb ribbon with respect to the span. Thus we can conclude that the homogenized constitutive law adequately represents the honeycomb sandwich core in bending as well. Validation of the homogenized material model under crushing and flexure enables its use in subsequent optimization of the honeycomb sandwich panels. The FORTRAN program is modified to handle the honeycomb material properties as design variables for the DE optimizer. This paves the way for simultaneous shape, size and core optimization for honeycomb sandwich panel.

Much of the work reported here is limited by high computation costs. Exploring the design space with a large number of design variables would require dedication of a large amount of computational resources over a significantly longer period of time. Improvements in optimizations strategies, especially better constraint handling, would help reduce this cost. Currently we are limited to exploring the domain of simple basis shapes with a handful of variables.

Future research is needed to optimize the *topology* of the honeycomb core, treating the density of each element as a design variable. Complex basis shapes might provide new concepts. Simultaneous optimization for ballistic protection and blast load mitigation needs further research. Blast related injuries are caused due to the magnitude of acceleration as well as its time duration. Established injury related parameters like Head Injury Criteria (HIC) and Chest Injury Criteria (CIC) can be considered as possible objective functions. Topology of the core in a sandwich panel for maximum energy absorption needs investigation.

References

1. Dharaneepathy, M.V. and Sudhesh, K. G., *Optimal Stiffening of Square Plates Subjected To Air-Blast Loading*, Computers & Structures. Vol.36,No.5, 891-899 (1990)
2. Xue, Z. and Hutchinson, J.W., *A Comparative study of impulse-resistant metal sandwich plates*, International Journal of Impact Engineering, Vol.30,No.10, 1283–1305 (2004)
3. Fleck, N.A. and Deshpande, V.S., *The Resistance of Clamped Sandwich Beams to Shock Loading*, vol. 71, J. of Applied Mechanics, Transactions of the ASME, Vol.71,No.3, 386-401, (2004)
4. Yen, C.F., Skaggs, R., Cheeseman, B.A., *Modeling of shock mitigation sandwich structures for blast protection*. The International Conference on Structural Stability and Dynamics, Kissimmee, Florida, June 19-22 (2005)
5. Main, J.A. and Gazonas, G.A, *Uniaxial crushing of sandwich plates under air blast: Influence of mass distribution*, International Journal of Solids and Structures, Vol.45, No.7-8, 2297–2321 (2008)
6. Argod, V., Belegundu, A.D., Aziz, A., Agarwala, V., Jain, R., and Rajan, S.D., *MPI-enabled Shape Optimization of Panels Subjected to Air Blast Loading*, International Journal of Simulation of Multidisciplinary Design Optimization, Vol.2, No.4, 273-282 (2008)
7. Argod, V., Nayak, S.K., Singh, A.K., Belegundu, A.D., *Shape Optimization Of Solid Isotropic Plates To Mitigate The Effects Of Air Blast Loading*, Mechanics Based Design of Structures and Machines, Vol.38, No.3, 362-371 (2010)
8. Wierzbicki., Tomasz., *Crushing analysis of metal honeycombs.* International Journal of Impact Engineering, Vol.1, No.2, 157-174 (1983)
9. Hexcel Corp., *Hexweb honeycomb attributes and properties.* (1999)
10. LS-DYNA Keyword Manual Version 971, Rev 5 (May 2010)
11. Nayak, S.K., *Optimization Of Honeycomb Core Sandwich Panel To Mitigate The Effects Of Air Blast Loading*, M.S. Thesis, The Pennsylvania State University, 8-22 (August 2010)
12. ASTM D 7250/D 7250M-06 *Standard Practice for Determining Sandwich Beam Flexural and Shear Stiffness*
13. ASTM C 393/C 393M-06 *Standard Test Method for Core Shear Properties of Sandwich Constructions by Beam Flexure*

14. Belegundu, A.D., Argod, V., Rajan, S.D., and Krishnan, K., *Shape Optimization of Panels Subject to Blast Loading Modeled with LS-DYNA,* 49th AIAA/ASME/ASCE/AHS/ASC Structures, Structural Dynamics, and Materials Conference, Schaumburg, Illinois, April 7-10 (2008)
15. Storn, R. and Price, K., *Differential Evolution a simple and efficient adaptive scheme for global optimization over continuous spaces,* Journal of Global optimization, 11, 341-359 (1997)